ACS APPLIED MATERIALS & INTERFACES

Research Article

www.acsami.org

Microwave Hydrothermal Transformation of Amorphous Calcium Carbonate Nanospheres and Application in Protein Adsorption

Chao Qi, Ying-Jie Zhu,* and Feng Chen

State Key Laboratory of High Performance Ceramics and Superfine Microstructure, Shanghai Institute of Ceramics, Chinese Academy of Sciences, Shanghai 200050, P. R. China

ABSTRACT: Calcium carbonate and calcium phosphate are the main components of biominerals. Among all of the forms of biominerals, amorphous calcium carbonate (ACC) and amorphous calcium phosphate (ACP) are the most important forms because they play a pivotal role in the process of biomineralization and are the precursors to the crystalline polymorphs. In this work, we first synthesized ACC in vitro using adenosine 5′-triphosphate disodium salt (ATP) as the stabilizer and investigated the transformation of the ACC under microwave hydrothermal conditions, and ACC/ACP composite nanospheres and carbonated hydroxyapatite (CHA) nanospheres were successfully prepared. In this novel strategy, ATP has two main functions: it serves as the stabilizer for ACC and the phosphorus source for ACP and CHA. Most importantly, the morphology and the size of the ACC precursor can be well-preserved after microwave heating, so it provides a new method for the preparation of calcium phosphate nanostructured materials using phosphorus-containing biomolecule-stabilized ACC as the precursor. Furthermore, the as-prepared ACC/ACP composite nanospheres have excellent biocompatibility and high protein adsorption capacity, indicating that they are promising for applications in biomedical fields such as drug delivery and protein adsorption.

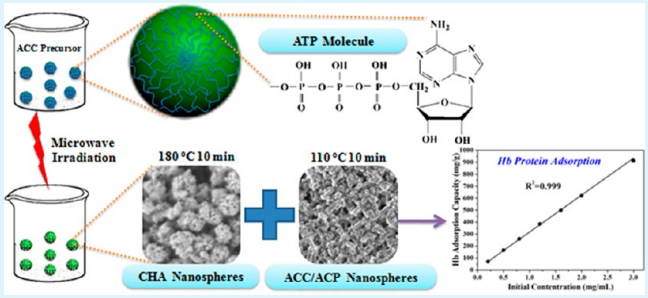

KEYWORDS: *microwave, calcium carbonate, calcium phosphate, hydroxyapatite, nanospheres, protein adsorption*

1. INTRODUCTION

Calcium carbonate and calcium phosphate, as the most significant biominerals naturally existing in biological systems,[1−4] have aroused enormous interest because they are widely used as a model system for studying biomimetic processes.[5−9] Organisms have the ability to use biomineralization to form composite materials such as skeletal, pearl, bone, and tooth, which are composed of calcium carbonate or calcium phosphate embedded in an organic matrix.[10−13] The process of biomineralization has inspired researchers to synthesize biogenic calcium carbonate and calcium phosphate in vitro using a biomimetic method. As ideal biomaterials because of their excellent biocompatibility, calcium carbonate and calcium phosphate have been investigated for applications in biomedical fields such as drug and gene delivery,[14−20] tissue engineering and bone repair,[21,22] and others.[23−26] In addition, calcium carbonate and calcium phosphate nanostructured materials are promising carriers for protein adsorption and release, which exhibit pH-responsive protein-release behavior;[27,28] thus, they have promising applications in various biomedical fields.

Among all of the forms of calcium carbonate and calcium phosphate, amorphous calcium carbonate (ACC) and amorphous calcium phosphate (ACP) are the most important phases because they play a pivotal role in the process of biomineralization for other phases and are the precursor to the crystalline polymorphs.[29−31] ACC has several potential biological functions, such as serving as a temporary storage deposit when needed because of its high solubility relative to the crystalline phases. Moreover, the bioavailability of ACC, commonly used medicinally as a calcium supplement or as an antacid, is roughly 40% more bioavailable than crystalline calcium carbonate, which is only around 20−30%.[32] However, compared with well-crystallized calcium phosphate, ACP is more bioactive, has better biodegradability, and can promote osteoblast adhesion and osteoconductivity.[33,34]

Despite the advantages of ACC and ACP, it is difficult to produce pure ACC and ACP without any stabilizer in vitro because of their low stability and high solubility and because they will crystallize rapidly to form one of the more stable polymorphs in aqueous solution.[35,36] However, ACC and ACP, stabilized by specific biological macromolecules,[37−40] have been found to exist widely in living organisms such as in ascidian skeleton, plant cystoliths, spicules from sponge, and mollusk shells.[41,42] Inspired by biomineralization, many researchers have been devoted to the design and synthesis of stabilized ACC and ACP using some additives such as biomolecules and organic molecules under mild conditions in vitro.[43−48] In addition, inorganic ions such as magnesium, phosphate, and silica also are capable of stabilizing ACC and ACP for a certain amount of time.[49−53] In spite of the progress that has been made, the

Received: December 31, 2013
Accepted: February 25, 2014
Published: February 25, 2014

Scheme 1. Schematic Illustration of the Transformation Process of ATP-Stabilized ACC Precursor under Microwave Hydrothermal Treatment

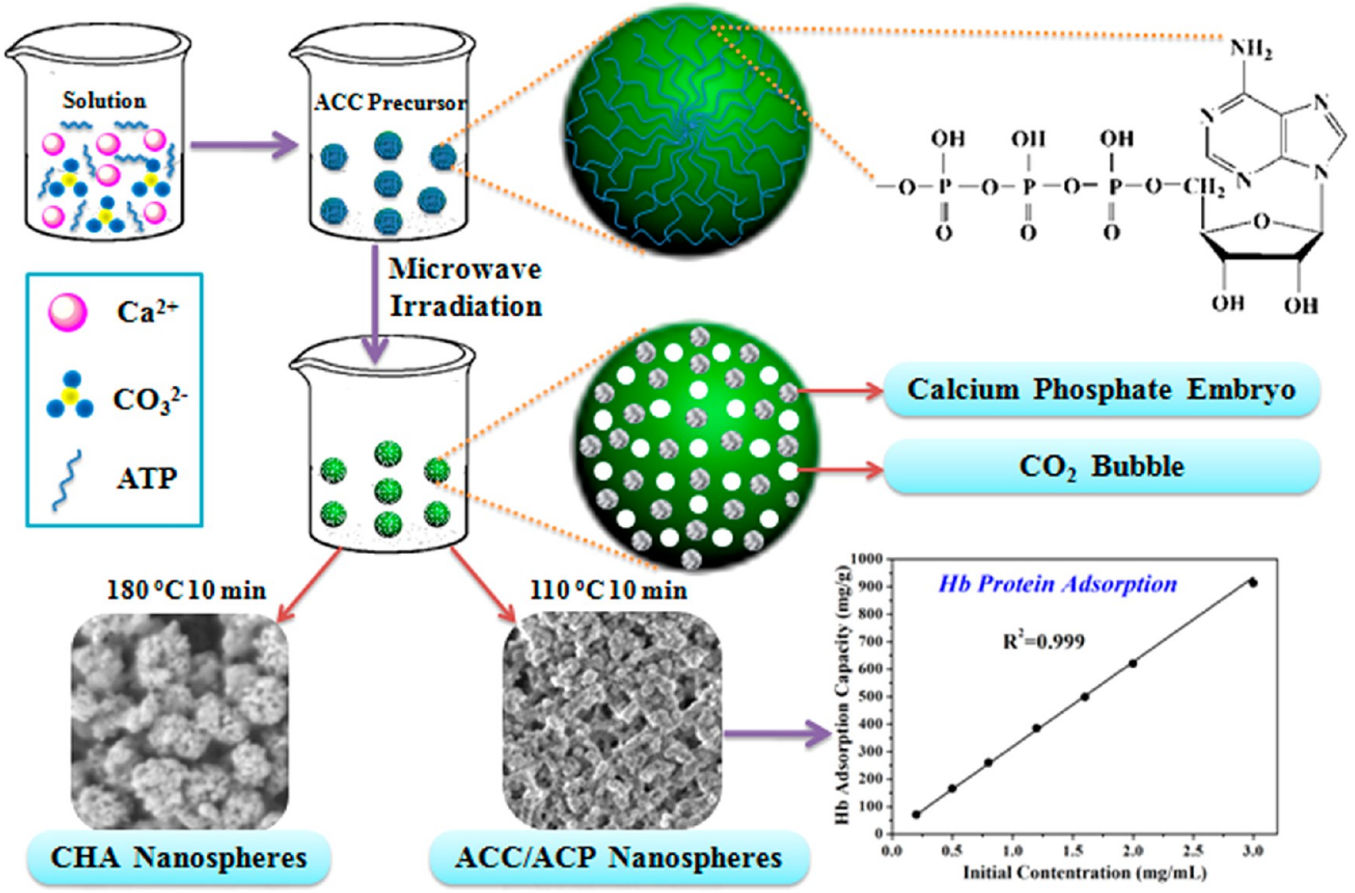

synthesis of stable ACC or ACP at a relatively high temperature still remains a challenge.

Since the first reports of microwave-assisted organic synthesis in 1986,[54,55] the application of microwave heating in synthetic chemistry and materials preparation has been a fast growing area of research. Microwave heating has many advantages compared with conventional heating methods, such as rapid volumetric heating, high reaction rate, time savings, lower energy consumption, and high efficiency.[56,57] Among these, the time savings and lower energy consumption of the microwave-assisted method are the most significant.

To understand the transformation process of ACC under microwave hydrothermal conditions, we synthesized ACC in vitro at room temperature using adenosine 5′-triphosphate disodium salt (ATP) as the stabilizer. ATP, as the most common energy carrier of the cell in biological systems, plays an important role in various life activities. Previous works indicate that ATP can strongly inhibit the formation of calcium carbonate crystals and induce deposition of amorphous calcium carbonate.[58] Moreover, ATP can be used as a stabilizer for ACP to inhibit the crystallization process in aqueous solution by poisoning heterogeneous nucleation sites and binding to an embryonic crystal nucleus to prevent its growth to a critical nucleus size.[53,59,60] Therefore, we used ATP biomolecules as a stabilizer to synthesize ACC in vitro at room temperature (Scheme 1). Then, we investigated the transformation process of the ACC under microwave hydrothermal conditions and successfully prepared ACC/ACP composite nanospheres and carbonated hydroxyapatite (CHA) nanospheres. In this strategy, ATP is used as the stabilizer for ACC and the phosphorus source for the formation of ACP and CHA. Moreover, the morphology and size of the ACC precursor can be well-preserved after microwave treatment, which provides a new method for the preparation of ACC/ACP composite nanostructured materials using ACC as the precursor, which is stabilized by phosphorus-containing biomolecules.

2. EXPERIMENTAL SECTION

2.1. Preparation of Stable ACC/ACP Composite Nanospheres. In a typical experiment for the synthesis of ACC/ACP composite nanospheres, 0.925 g of $CaCl_2$ was dissolved in 250 mL of deionized water to form solution A, and 1.060 g of Na_2CO_3 was dissolved in 100 mL of deionized water to form solution B. After 0.110 g of ATP was added into 30 mL of solution A and the pH value was adjusted to 9 using 1 M NaOH, 10 mL of solution B was added dropwise to solution A under magnetic stirring, and the pH value was maintained at 9. The final concentrations of the resulting suspension were $CaCl_2$, 25 mM; Na_2CO_3, 25 mM; and ATP, 5 mM. The resulting suspension was stirred at room temperature for 1 h, loaded into a 60 mL autoclave, sealed, microwave-heated in a microwave oven (MDS-6, Sineo, China) to 110 °C, maintained at this temperature for 10 min, and then cooled naturally to room temperature. The product was separated by centrifugation, washed with deionized water and ethanol several times, and dried at 60 °C for 24 h. Other samples were prepared by similar procedures but with varying experimental parameters (see Table 1 for details of the preparation conditions). All of the chemicals used in the sample preparation were analytical grade and were purchased and used as received without further purification.

dx.doi.org/10.1021/am4060645 | ACS Appl. Mater. Interfaces 2014, 6, 4310−4320

2.2. Characterization. X-ray powder diffraction (XRD) patterns were recorded by using a X-ray diffractometer (Rigaku D/max 2550 V, Cu Kα, λ = 1.54178 Å). Fourier-transform infrared (FTIR) spectra were taken on a FTIR spectrometer (FTIR-7600, Lambda Scientific, Australia). Scanning electron microscopy (SEM) images were recorded with a field-emission scanning electron microscope (Hitachi S-4800, Japan). Transmission electron microscopy (TEM) images were recorded with a transmission electron microscope (Hitachi H-800, Japan). The Brunauer–Emmett–Teller (BET) specific surface area and pore-size distribution were measured with a specific surface area and pore-size analyzer (V-sorb 2800P, Gold APP Instruments, China). The thermogravimetric (TG) and differential scanning calorimetry (DSC) curves were measured on a STA 409/PC simultaneous thermal analyzer (Netzsch, Germany) with a heating rate of 10 °C min^{-1} in flowing air. The ATP and hemoglobin (Hb) concentrations were analyzed using a UV–vis spectrophotometer (UV-2300, Techcomp) at wavelengths of 258 and 405 nm, respectively. Ca and P elemental contents were measured using an inductively coupled plasma (ICP) optical emission spectrometer (JY 2000-2, Horiba, France). The zeta potentials were measured with a zeta-potential analyzer (ZetaPlus, Brookhaven Instruments Corporation).

2.3. Determination of ATP Content and Ca/P Molar Ratio. Ten milligrams of powdered sample was immersed in a 0.1 M HCl solution (5 mL) and shaken at a constant rate for 4 h at 37 °C to dissolve the sample completely. The clear solution was measured by ICP to determine the Ca/P molar ratio and by UV–vis absorption to determine the ATP content.

2.4. ACC/ACP Composite Nanospheres Dissolution Experiment. The powder of the ACC/ACP composite nanospheres (30 mg) was immersed in 30 mL of phosphate-buffered saline (PBS) solution with different pH values (pH 7.4, 6.0, or 5.0) at 37 °C with constant shaking (120 rpm). The supernatant solution (1 mL) was withdrawn for ICP analysis and UV–vis absorption analysis to measure the concentration of Ca^{2+} ions and ATP at given time intervals and was replaced with the fresh PBS with the same volume and the same pH value (37 °C, pH 7.4, 6.0, or 5.0). Then, the product was separated by centrifugation after soaking in the PBS solution for 12 days and dried at 60 °C for 24 h for XRD analysis.

2.5. Transformation of ACC/ACP Composite Nanospheres in PBS Solution. The powdered sample (18 mg) was immersed in 9 mL of PBS solution (pH 7.4) for different times at 37 °C under constant shaking (120 rpm), separated by centrifugation, washed with deionized water and ethanol once, and dried at 60 °C for 24 h for XRD and FTIR analysis.

2.6. In Vitro Cytotoxicity Tests. Human gastric carcinoma cells (MGC-803) were cultured in RPMI-1640 medium supplemented with 10% fetal bovine serum (FBS) and 1% penicillin–streptomycin at 37 °C for 48 h. Then, the cells were seeded in 96-well flat-bottom microassay plates at a concentration of 1×10^4 cells per milliliter and cultured for 24 h. The sterilized powder of ACC/ACP composite nanospheres was added into the wells at concentrations ranging from 0.1–100 μg mL^{-1} and cocultured with the cells for 48 h. The sample-free tissue culture plate was used as a control. Cell viability was quantified by 3-(4,5-dimethylthiazol-2-yl)-2,5-diphenyltetrazolium bromide (MTT) assay. The data represents the mean value of three parallel measurements.

2.7. In Vitro Protein Adsorption. Hemoglobin (Hb, molecular weight ~64 500 Da) was chosen as a model protein for the investigation. The protein adsorption experiments at different protein concentrations were performed as follows. Powdered ACC/ACP composite nanospheres (5 mg each) were immersed in aqueous solutions that contained various concentrations of the protein (2 mL, 0–3.0 mg mL^{-1}). After ultrasonic treatment for 15 min, each solution was shaken at a constant rate for 4 h at 37 °C. Then, the solution was centrifuged, and the amount of protein in the supernatant was measured by UV–vis absorption at a wavelength of 405 nm.

2.8. In Vitro Protein Release. For the in vitro protein release from the ACC/ACP protein-adsorption system, the powdered ACC/ACP composite nanospheres (100 mg) were immersed in an aqueous solution of Hb (3 mg mL^{-1}, 6 mL). After ultrasonic treatment for 15 min, the solution was continuously shaken in a sealed vessel at 37 °C for 4 h followed by centrifugation and freeze-drying to obtain the protein-adsorbed ACC/ACP composite nanospheres. The in vitro protein-release experiments at different pH values were performed as follows. The powdered ACC/ACP composite nanosphere protein-adsorption system (20 mg) was immersed in PBS solution (30 mL) at different pH values (pH 7.4, 6.0, or 5.0) at 37 °C with constant shaking (120 rpm). The protein-release solution (1 mL) was withdrawn for UV–vis absorption analysis at given time intervals and replaced with the same volume and the same pH value of fresh PBS (37 °C).

3. RESULTS AND DISCUSSION

3.1. Synthesis of ACC Nanospheres Precursor. To study the transformation process of ACC under a microwave hydrothermal conditions, we first synthesized ACC in vitro at room temperature using ATP as the stabilizer. The XRD pattern in Figure 1a shows no obvious diffraction peaks,

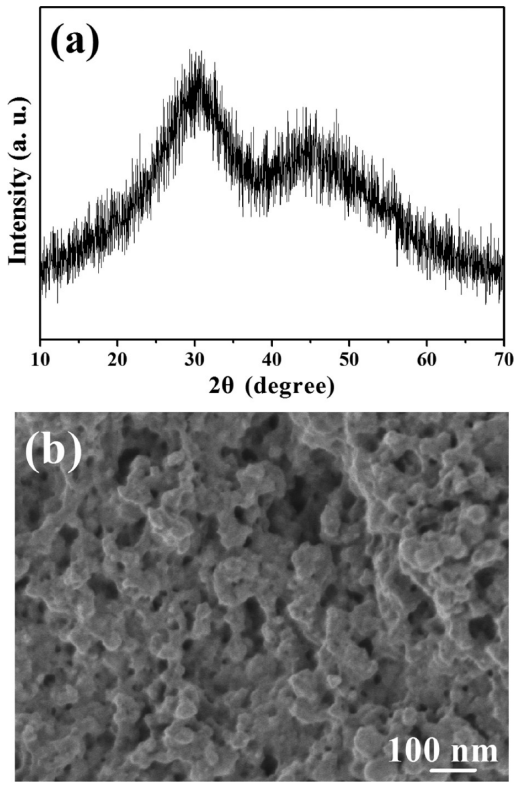

Figure 1. XRD pattern (a) and SEM micrograph (b) of ACC nanospheres stabilized by ATP.

indicating that the sample prepared with ATP at room temperature was an amorphous phase. The morphology (Figure 1b) of the sample consisted of ACC nanospheres with diameters of about 50 nm.

3.2. Transformation of ACC Nanospheres under Microwave Irradiation. Figure 2 shows the phase transformation of the ACC amorphous nanospheres as the precursor after the microwave hydrothermal treatment at different temperatures for different times. When the microwave hydrothermal temperature was low and the time was short (110 °C for 10 min), the product still consisted of an amorphous phase (Figure 2a). The ATP absorbance (Figure 3) after the microwave hydrothermal treatment of the ACC precursor decreased compared with that of the untreated

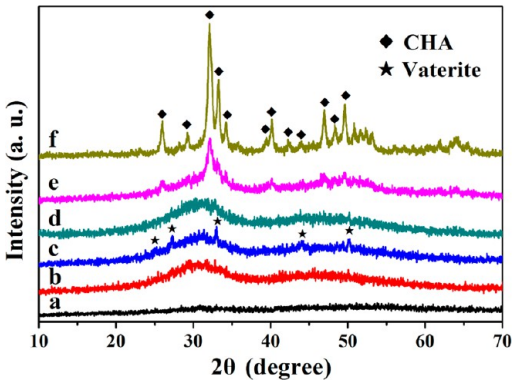

Figure 2. XRD patterns of the products obtained by microwave hydrothermal treatment of the ATP-stabilized ACC nanospheres at different temperatures for different times: (a) 110 °C, 10 min; (b) 110 °C, 30 min; (c) 110 °C, 60 min; (d) 130 °C, 10 min; (e) 150 °C, 10 min; and (f) 180 °C, 10 min.

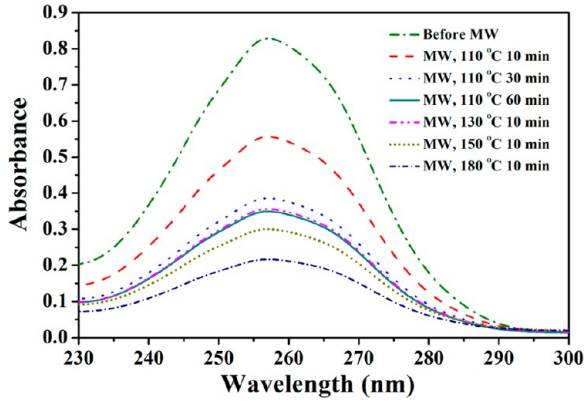

Figure 3. UV−vis absorption spectra after the samples were completely dissolved in 0.1 M HCl. The samples were prepared before and after microwave hydrothermal treatment at different temperatures for different times.

sample, and there was no obvious change in the Ca/P molar ratio before and after microwave hydrothermal treatment (Table 1), indicating that some ATP molecules were hydrolyzed to form ACP, so the composition of this sample is ACC and ACP composite materials (ACC/ACP). It is worth noting that the remnant ATP molecules can stabilize ACC and ACP even at a relatively high temperature. By further prolonging the microwave hydrothermal time or increasing the temperature, the ATP absorbance of the products gradually decreased, indicating that more ATP molecules were hydrolyzed, and the product gradually crystallized and contained a small amount of vaterite (Figure 2c) because there were not enough ATP molecules to stabilize the ACC/ACP composite materials. The higher the microwave hydrothermal temperature, the more ATP molecules hydrolyze and the more crystallization of the product occurs. When the temperature was elevated to 180 °C for 10 min, the product was completely crystallized to form carbonated hydroxyapatite (CHA) nanospheres (Figure 2f).

To further investigate the composition change of the samples that were prepared using ACC as the precursor by the microwave hydrothermal method, the FTIR spectra of the samples were measured. The FTIR spectra in Figure 4 indicate

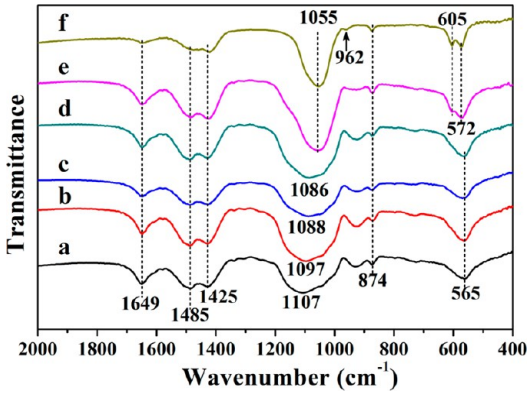

Figure 4. FTIR spectra of the samples obtained by microwave hydrothermal treatment of the ATP-stabilized ACC precursor at different temperatures for different times: (a) 110 °C, 10 min; (b) 110 °C, 30 min; (c) 110 °C, 60 min; (d) 130 °C, 10 min; (e) 150 °C, 10 min; and (f) 180 °C, 10 min.

that the samples obtained by microwave hydrothermal treatment exhibited split peaks of the ν_3 absorption band at 1485 and 1425 cm^{-1} as well as a strong ν_2 (out-plane bending of CO_3^{2-}) absorption band at 874 cm^{-1}; these peaks are the characteristic absorption bands of CO_3^{2-}.[61,62] Moreover, with prolonged microwave hydrothermal time or the temperature, the broad PO_4^{3-} absorption band located at 1107 cm^{-1} gradually red-shifted. When the microwave hydrothermal temperature was 180 °C, the absorption peak at 565 cm^{-1}, referring to the ν_4 bending mode of the O−P−O bond, split into two peaks at 605 and 572 cm^{-1}, and the absorption peak at 962 cm^{-1} is ascribed to the ν_1 stretching mode of the P−O bond of the phosphate group; these bands are the characteristic absorption bands of hydroxyapatite,[63] so the FTIR result is consisted with the XRD analysis.

The morphologies of the samples obtained by the microwave hydrothermal treatment of the ACC precursor at different temperatures for different times were observed by SEM (Figure 5) and TEM (Figure 6). The experiments showed that no obvious change was observed in the morphology and the size of the samples after the microwave hydrothermal treatment at

Table 1. Experimental Conditions for the Preparation of Typical Samples and Their Ca/P Molar Ratio and ATP Content

sample no.	temperature (°C)	time (min)	content of ATP (wt %)	Ca/P molar ratio
ACC precursor			49.565	1.708
a	110	10	25.084	1.647
b	110	30	20.123	1.612
c	110	60	17.699	1.816
d	130	10	17.883	1.699
e	150	10	14.848	2.145
f	180	10	10.490	1.930

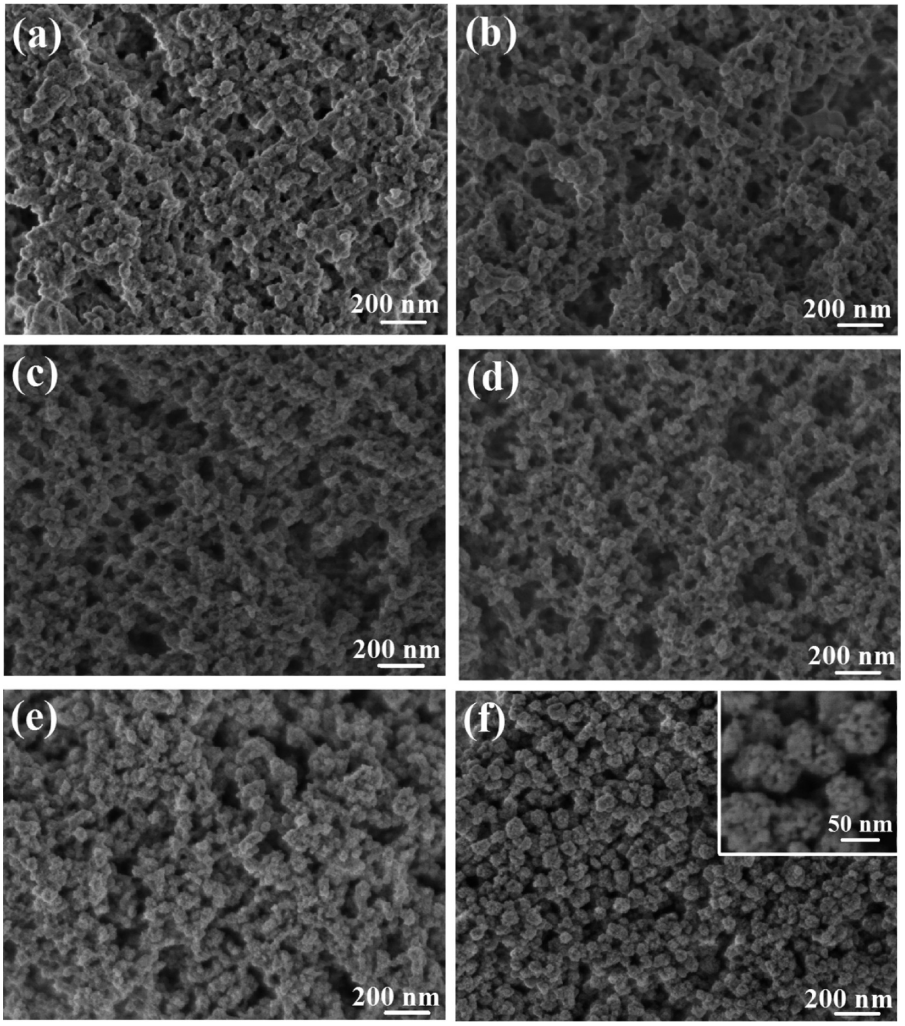

Figure 5. SEM micrographs of the products obtained by the microwave hydrothermal treatment of the ATP-stabilized ACC precursor at different temperatures for different times: (a) 110 °C, 10 min; (b) 110 °C, 30 min; (c) 110 °C, 60 min; (d) 130 °C, 10 min; (e) 150 °C, 10 min; and (f) 180 °C, 10 min.

different temperatures for different times. The size distribution of the ACC/ACP nanospheres prepared by the microwave hydrothermal treatment of the ATP-stabilized ACC precursor at 110 °C for 10 min was measured by dynamic light scattering (DLS), and the result is shown in Figure 7. From Figure 7, it can be seen that the ACC/ACP nanospheres had a narrow size distribution, with an average diameter of 227 nm. The selected-area electron diffraction (SAED) pattern of the samples treated at 110 °C exhibited no obvious distinct diffraction spots, indicating that they were amorphous. However, when the microwave hydrothermal temperature was increased to 180 °C, the sample was composed of porous CHA nanospheres with diameters of about 50 nm, these CHA nanospheres were formed by self-assembly of CHA nanopaticles, and the electron diffraction rings indicate that the sample was polycrystalline. These results are consistent with the XRD analysis, but they are different from our previous work on the synthesis of hydroxyapatite nanowires using ATP as a phosphorus source at a relatively high microwave hydrothermal temperature.[64] Therefore, using ACC as the precursor, which was stabilized by phosphorus-containing biomolecules, can allow for the synthesis of calcium carbonate/calcium phosphate composite nanostructured materials, and the morphology and size of the ACC precursor can be well-preserved after the microwave hydrothermal treatment.

The thermal stability of the samples prepared by microwave hydrothermal treatment of the ATP-stabilized ACC precursor at different temperatures for different times was analyzed by TG (Figure 8) and DSC (Figure 9). The TG curves of the samples can be divided into three stages. The weight loss below 200 °C is assigned to the absorbed water and the structural water, which widely exists in an amorphous phase. The decomposition temperature of ATP molecules is above 200 °C, so the weight loss between 200 and 450 °C is attributed to the decomposition of ATP molecules. When the temperature is higher than 450 °C, the weight loss is mainly assigned to the decomposition of calcium carbonate, and the complete decomposition of calcium carbonate is below 800 °C. The DSC curve of the sample prepared at 110 °C for 10 min showed a sharp exothermic peak at 705 °C, which is due to the crystallization process of the amorphous phase. By increasing the microwave hydrothermal time or temperature, this exothermic peak gradually weakened, indicating that the proportion of the amorphous phase in the sample gradually decreased. For the sample prepared at 180 °C for 10 min, the

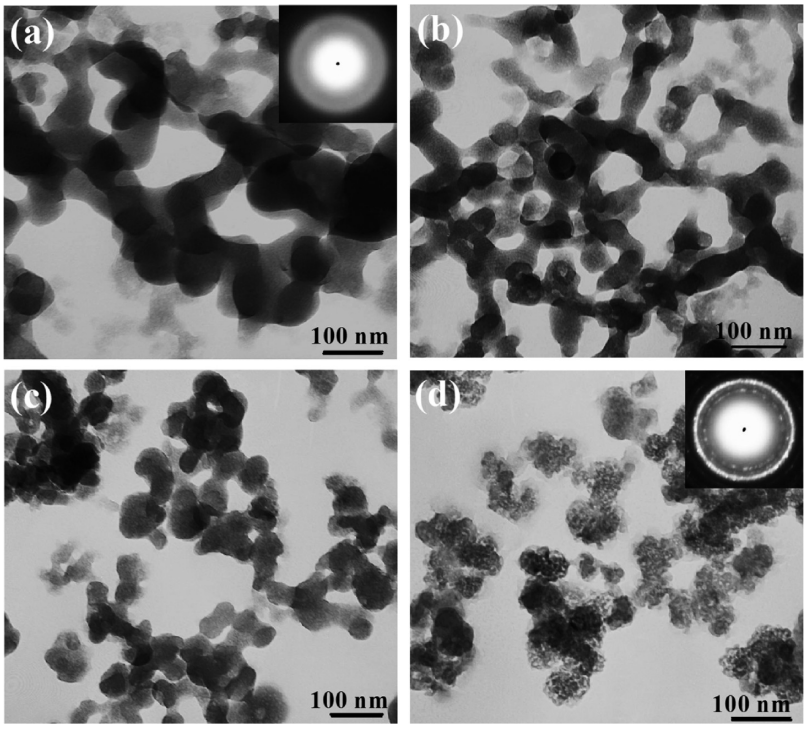

Figure 6. TEM micrographs of the products obtained by the microwave hydrothermal treatment of the ATP-stabilized ACC precursor at different temperatures for different times: (a) 110 °C, 10 min; (b) 110 °C, 60 min; (c) 150 °C, 10 min; and (d) 180 °C, 10 min.

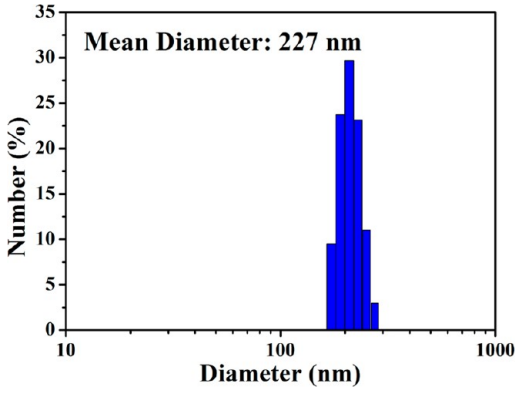

Figure 7. Size distribution of ACC/ACP composite nanospheres synthesized by the microwave hydrothermal treatment of the ATP-stabilized ACC precursor at 110 °C for 10 min measured by dynamic light scattering in water.

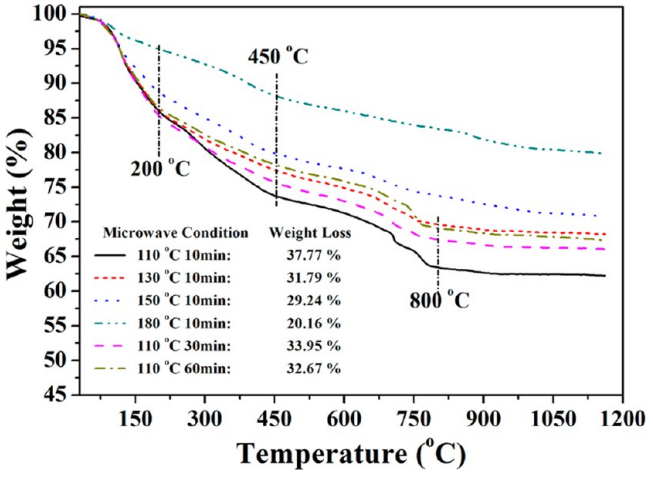

Figure 8. TG curves of the samples prepared by the microwave hydrothermal treatment of the ATP-stabilized ACC precursor at different temperatures for different times.

exothermic peak disappeared because there was no amorphous phase in this sample.

We measured the specific surface area of the ACC/ACP composite nanospheres prepared at 110 °C for 10 min using a N_2 adsorption–desorption isotherm (Figure 10). The BET specific surface area (S_{BET}) and the corresponding Barett–Joyner–Halenda (BJH) desorption cumulative pore volume (V_P) of the ACC/ACP composite nanospheres was 141.3 m^2 g^{-1} and 1.5 cm^3 g^{-1}, respectively. The relatively large S_{BET} and V_P values are favorable for the application of these nanospheres in protein adsorption because they provide ideal adsorption sites and physical space for protein molecules. Moreover, the BJH desorption pore-size distribution curve (Figure 10b) shows two main pore sizes of 5.4 and 66 nm, and the average pore size was 32.5 nm. The small pore-size distribution peak is caused by the carbon dioxide bubbles formed during the transformation process of part of ACC to ACP, whereas the large pore-size distribution peak is formed by the aggregation of ACC/ACP nanospheres.

3.3. Transformation of ACC/ACP Composite Nanospheres in PBS Solution. To investigate the stability of the ACC/ACP composite nanospheres, the sample prepared by the microwave hydrothermal treatment of ATP-stabilized ACC nanospheres at 110 °C for 10 min was soaked in PBS solutions with different pH values. The Ca^{2+} ion dissolution rate, which represents the degradation of the sample, has an obvious pH-dependent behavior: the lower the pH value, the higher the cumulative dissolution percentage. At pH 7.4, the cumulative percentage of the dissolved Ca^{2+} ions reaches a balance at about 10% (Figure 11a), indicating that the as-prepared ACC/ACP

dx.doi.org/10.1021/am4060645 | ACS Appl. Mater. Interfaces 2014, 6, 4310–4320

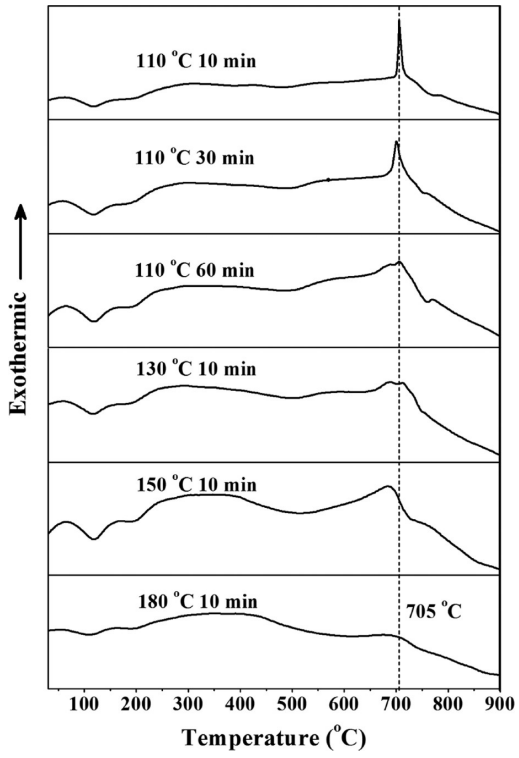

Figure 9. DSC curves of the samples prepared by the microwave hydrothermal method at different temperatures for different times using ATP-stabilized ACC nanospheres as the precursor.

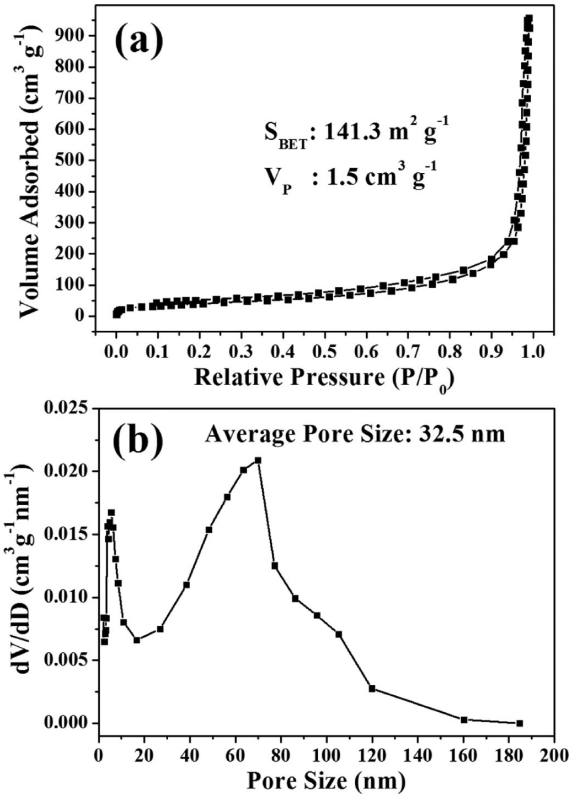

Figure 10. N_2 adsorption−desorption isotherm (a) and BJH desorption pore-size distribution cure (b) of the ACC/ACP composite nanospheres prepared by the microwave hydrothermal treatment of ATP-stabilized ACC nanospheres at 110 °C for 10 min.

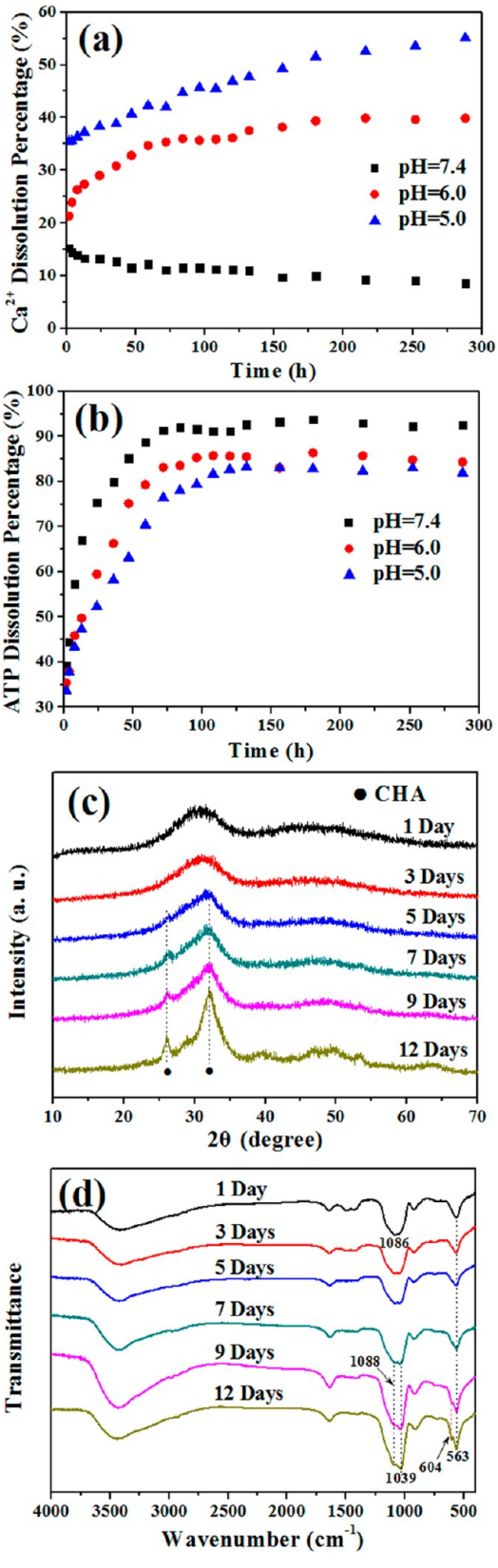

Figure 11. Cumulative dissolution percentage of ACC/ACP composite nanospheres after soaking in PBS solutions with different pH values for different times: (a) Ca^{2+} ions and (b) ATP molecules. (c) XRD patterns and (d) FTIR spectra of ACC/ACP composite nanospheres after soaking in PBS solution (pH 7.4) for different times.

dx.doi.org/10.1021/am4060645 | ACS Appl. Mater. Interfaces 2014, 6, 4310−4320

composite nanospheres have a certain stability at this pH value, whereas at the pH 6.0 and 5.0, the cumulative percentage of the dissolved Ca^{2+} ions increased with the soaking time. However, the cumulative percentage of the dissolved ATP molecules (Figure 11b) has an opposite trend compared with the cumulative percentage of the dissolved Ca^{2+} ions at different pH values: the higher the pH value, the higher the dissolution percentage of ATP. This phenomenon can be explained by the fact that the pH value can affect the charge of ATP molecules, changing the electrostatic interaction between ATP molecules and ACC/ACP composite nanospheres. Moreover, the cumulative percentage of the dissolved ATP molecules can reach a balance within about 100 h at different pH values. After soaking in PBS solution (pH 7.4) for 12 days, the XRD pattern (Figure 11c) and the FTIR spectrum (Figure 11d) indicate that ACC/ACP composite nanospheres partly transformed to CHA.

To further study the transformation process of ACC/ACP composite nanospheres in the PBS solution, we performed XRD and FTIR measurements of the samples after soaking in PBS solution (pH 7.4) for different times, as shown in Figure 11c,d. The XRD pattern (Figure 11c) shows that small diffraction peaks of CHA appeared in the XRD pattern of the sample after soaking in PBS solution (pH 7.4) for 5 days, indicating that a small amount of CHA formed on the surface of ACC/ACP composite nanospheres by the reaction of dissolving Ca^{2+} ions with CO_3^{2-} and PO_4^{3-} ions (from the PBS solution). The K_{sp} of calcium phosphate (2.07×10^{-29}) is much lower than that of calcium carbonate (2.8×10^{-9}), so the formation of calcium phosphate is reasonable. With increasing soaking time, the intensities of diffraction peaks of CHA gradually increased, indicating the formation of more CHA. On one hand, the formation of CHA needed to consume a certain amount of Ca^{2+} ions; on the other hand, the formation of a new CAP layer on the surface of ACC/ACP composite nanospheres inhibited the further dissolution of Ca^{2+} and CO_3^{2-} ions.

The FTIR spectra (Figure 11d) show that the PO_4^{3-} absorption band located at around 1086 cm^{-1} split into two peaks at 1088 and 1039 cm^{-1} after soaking in the PBS solution for 7 days, indicating that part of ACC transformed to calcium phosphate. With increasing soaking time, the PO_4^{3-} absorption band located at 563 cm^{-1} further split into two peaks at 604 and 563 cm^{-1}, indicating that more ACC transformed to calcium phosphate. The content of ATP in the ACC/ACP nanocomposite sample was lower than that of the ACC precursor (Table 1), so there was not enough ATP to inhibit the formation of calcium phosphate after soaking in the PBS solution, and the stable ACC/ACP composite nanospheres could maintain the amorphous phase in the PBS solution for only 5 days. These results indicate that ATP biomolecules can be used as an excellent stabilizer for amorphous biomaterials and can inhibit the transformation from the amorphous phase to the crystalline phase, which is important for the investigation of the biomineralization process.

3.4. Protein Adsorption and in Vitro Protein Release. Calcium carbonate and calcium phosphate are ideal biomaterials because of their excellent biocompatibility, and they have been investigated for use in pH-responsive drug release for cancer treatment. Herein, we investigated the protein-adsorption and -release performance of the as-prepared ACC/ACP composite nanospheres using hemoglobin (Hb) as a model protein. Cytotoxicity tests of the ACC/ACP composite nanospheres were performed using human gastric carcinoma cells (MGC-803), which showed no appreciable toxicity when the cells were cocultured with ACC/ACP composite nanospheres at concentrations in the range 0.1–100 $\mu g\ mL^{-1}$ (Figure 12a), so ACC/ACP composite nanospheres are promising for applications in the biomedical field. The high biocompatibility can be explained by the chemical nature of the as-prepared ACC/ACP composite nanospheres.

The adsorption of Hb in the ACC/ACP composite nanospheres was investigated at different initial concentrations of Hb. As shown in Figure 12b, the amount of adsorbed Hb on the ACC/ACP composite nanospheres increased with the increasing initial concentration of Hb in the range 0–3.0 mg mL^{-1} and reached 913 mg g^{-1} at a Hb concentration of 3.0 mg mL^{-1}, which is much higher than that of the pure calcium phosphate protein-adsorption system.[28,65] Moreover, the Hb adsorption capacity of the ACC/ACP composite nanospheres has a good linear relationship with the Hb initial concentration (Figure 12c). The ACC/ACP composite nanospheres still did not reach saturated adsorption at a high Hb concentration (3.0 mg mL^{-1}), indicating that they have a high protein-adsorption capacity. It should be noted that the Hb adsorption percentage decreased sharply with increasing the initial Hb concentration in the low range and decreased slowly in the high initial Hb concentration range (Figure 12d).

In addition, the Hb release performance of the ACC/ACP composite nanosphere protein-adsorption system was investigated. It was found that the released amount of Hb from the ACC/ACP composite nanosphere protein-adsorbption system in PBS solution was dependent on the pH, and the cumulative amount of released Hb decreased with decreasing pH (Figure 13). This result may be explained by the electrostatic interaction between Hb molecules and the ACC/ACP composite nanospheres. In general, the isoelectric point (pI) of Hb is within the range 6.8–7.0.[66] When the pH value of the PBS solution is below the pI value of Hb, the Hb molecules will become positively charged, whereas when the pH value is higher than the pI value, the Hb molecules will become negatively charged. As shown in Figure 14, the zeta potential of ACC/ACP composite nanospheres was negative in PBS solutions with different pH values of 7.4, 6.0, and 5.0, indicating that the ACC/ACP composite nanospheres were negatively charged in PBS solutions with different pH values of 7.4, 6.0, and 5.0. For Hb molecules, the zeta potential was negative at pH 7.4; however, it became positive at pH 6.0 and 5.0, implying that Hb molecules were negatively charged in PBS solution at pH 7.4 and positively charged at pH 6.0 and 5.0. Thus, when the pH of the PBS solution was 7.4, both the Hb molecules and the ACC/ACP composite nanospheres were negatively charged and the electrostatic repulsion effect accelerated the Hb release from the ACC/ACP composite nanosphere protein-adsorption system. When the pH was 6.0 and 5.0, the Hb molecules became positively charged and the electrostatic attraction effect restrained the release of Hb: the lower the pH value, the stronger the electrostatic interaction and the slower the release of Hb. This result is consistent with our previous report on Hb adsorption onto hydroxyapatite hollow microspheres.[28,65] However, according to the results shown in Figure 11a, the ACC/ACP composite nanospheres are partly dissolved in PBS solutions at low pH values, leading to the acceleration of Hb release from the ACC/ACP composite nanospheres. The ACC/ACP composite nanospheres had a high-protein-adsorption capacity that still did not reach saturated adsorption at a Hb concentration of 3.0 mg mL^{-1} (Figure 12). Although

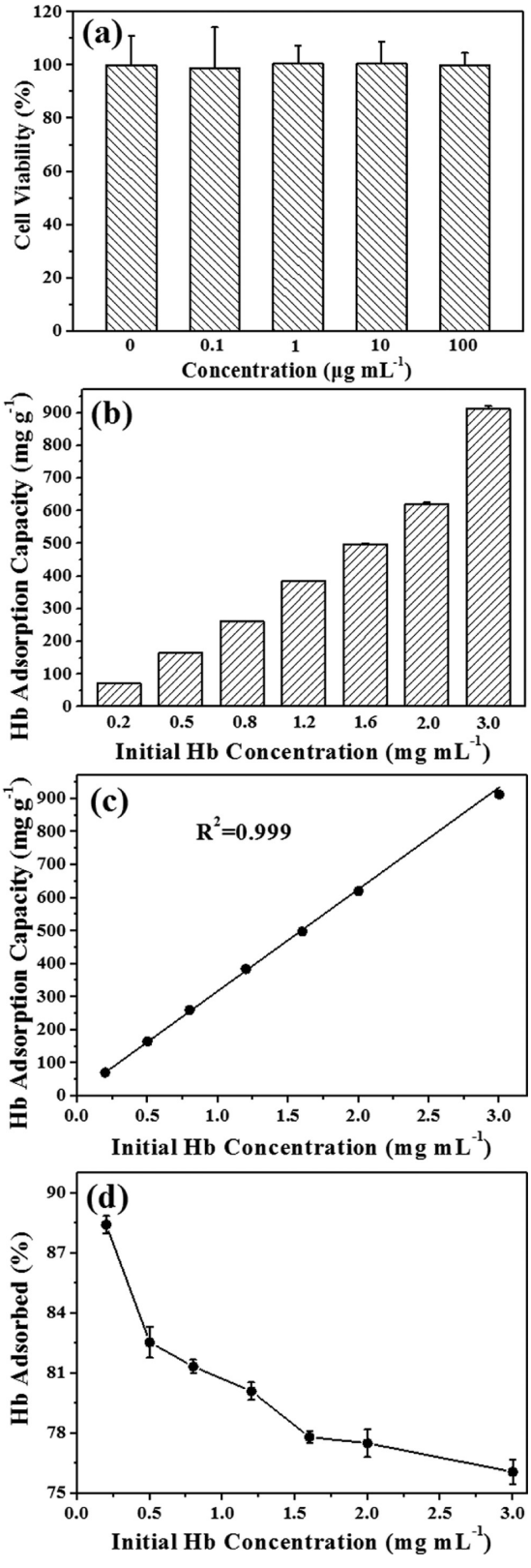

Figure 12. (a) Cytotoxicity tests of human gastric carcinoma cells (MGC-803). (b) Hb adsorption capacities at different initial concentrations of Hb, (c) Hb adsorption capacity as a liner function of Hb initial concentration, and (d) Hb adsorption percentage as a function of Hb initial concentration. The ACC/ACP composite nanospheres used in these experiments were prepared by the microwave hydrothermal treatment of ATP-stabilized ACC nanospheres at 110 °C for 10 min.

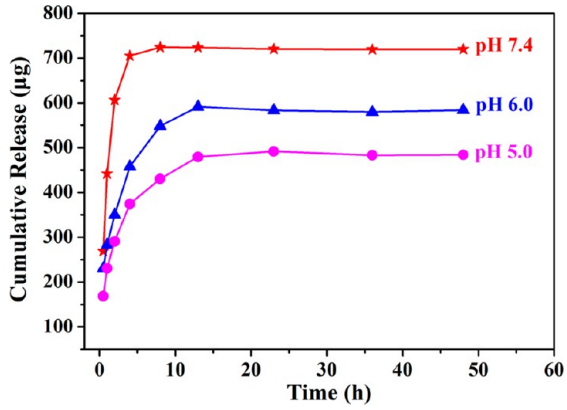

Figure 13. Hb release curve of the ACC/ACP composite nanosphere protein-adsorption system in PBS solutions with different pH values.

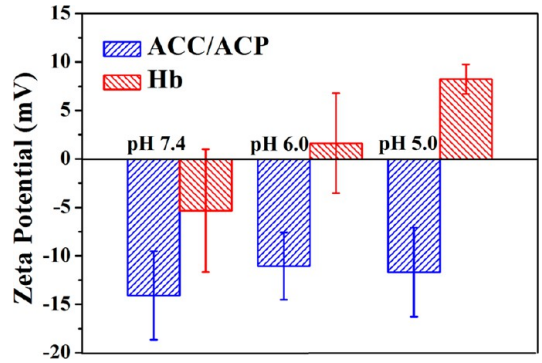

Figure 14. Zeta potentials of ACC/ACP composite nanospheres and Hb in PBS solution at different pH values.

the dissolution of a small amount of ACC/ACP composite nanospheres had some effect on the Hb release performance, the difference in the Hb release performance in PBS solutions with different pH values was mainly caused by the electrostatic interaction between Hb molecules and the ACC/ACP composite nanospheres.

4. CONCLUSIONS

We have successfully prepared ACC/ACP composite nanospheres with uniform size by using ACC that was stabilized by ATP as the precursor, and we investigated the transformation process of ACC under microwave hydrothermal conditions. In this strategy, ATP was used as both the stabilizer of ACC and the phosphorus source for ACP. Moreover, the carbon dioxide discharge during the decomposition of the ACC precursor can be used as a very good pore-forming agent to synthesize a porous material. Most interesting is that the morphology and size of the ACC precursor remained after microwave treatment, which provides a new method for the preparation of ACC/ACP composite nanomaterials using ACC stabilized by a phosphorus-containing biomolecule as the precursor. Furthermore, the stable ACC/ACP composite nanospheres can maintain the amorphous phase after soaking in PBS solution for 5 days because the ATP molecule dissolved from the sample and prevented the crystallization; this result indicated that ATP can prevent the transformation of a biomineral from an amorphous phase to a crystal phase, which is important for investigating a biomineralization process. Importantly, the good biocompatibility and high protein-adsorption capacity of the ACC/ACP composite nanospheres showed that they are promising for

applications in biomedical fields such as drug delivery and protein adsorption.

AUTHOR INFORMATION

Corresponding Author

*Tel: 0086-21-52412616; Fax: 0086-21-52413122; E-mail: y.j.zhu@mail.sic.ac.cn.

Author Contributions

The manuscript was written through contributions of all authors. All authors have given approval to the final version of the manuscript.

Notes

The authors declare no competing financial interest.

ACKNOWLEDGMENTS

Financial support from the National Natural Science Foundation of China (nos. 51172260 and 51121064), the National Basic Research Program of China (973 Program, no. 2012CB933600), and the Science and Technology Commission of Shanghai (nos. 11nm0506600 and 11nm0503600) is gratefully acknowledged.

REFERENCES

(1) Addadi, L.; Raz, S.; Weiner, S. Taking Advantage of Disorder: Amorphous Calcium Carbonate and Its Roles in Biomineralization. *Adv. Mater.* **2003**, *15*, 959−970.

(2) Raiteri, P.; Gale, J. D. Water Is the Key to Nonclassical Nucleation of Amorphous Calcium Carbonate. *J. Am. Chem. Soc.* **2010**, *132*, 17623−17634.

(3) Dorozhkin, S. V. Calcium Orthophosphates in Nature, Biology and Medicine. *Materials* **2009**, *2*, 399−498.

(4) Dorozhkin, S. V. Calcium Orthophosphates. *J. Mater. Sci.* **2007**, *42*, 1061−1095.

(5) Gal, A.; Habraken, W.; Gur, D.; Fratzl, P.; Weiner, S.; Addadi, L. Calcite Crystal Growth by a Solid-State Transformation of Stabilized Amorphous Calcium Carbonate Nanospheres in a Hydrogel. *Angew. Chem., Int. Ed.* **2013**, *52*, 4867−4870.

(6) Wang, Y. W.; Kim, Y. Y.; Stephens, C. J.; Meldrum, F. C.; Christenson, H. K. In Situ Study of the Precipitation and Crystallization of Amorphous Calcium Carbonate (ACC). *Cryst. Growth Des.* **2012**, *12*, 1212−1217.

(7) Bots, P.; Benning, L. G.; Rodriguez-Blanco, J.-D.; Roncal-Herrero, T.; Shaw, S. Mechanistic Insights into the Crystallization of Amorphous Calcium Carbonate (ACC). *Cryst. Growth Des.* **2012**, *12*, 3806−3814.

(8) Kimura, T.; Koga, N. Monohydrocalcite in Comparison with Hydrated Amorphous Calcium Carbonate: Precipitation Condition and Thermal Behavior. *Cryst. Growth Des.* **2011**, *11*, 3877−3884.

(9) Palmer, L. C.; Newcomb, C. J.; Kaltz, S. R.; Spoerke, E. D.; Stupp, S. I. Biomimetic Systems for Hydroxyapatite Mineralization Inspired by Bone and Enamel. *Chem. Rev.* **2008**, *108*, 4754−4783.

(10) Wehrmeister, U.; Jacob, D. E.; Soldati, A. L.; Loges, N.; Häger, T.; Hofmeister, W. Amorphous, Nanocrystalline and Crystalline Calcium Carbonates in Biological Materials. *J. Raman Spectrosc.* **2011**, *42*, 926−935.

(11) Foran, E.; Weiner, S.; Fine, M. Biogenic Fish-Gut Calcium Carbonate Is a Stable Amorphous Phase in the Gilt-Head Seabream, *Sparus aurata*. *Sci. Rep.* **2013**, *3*, 1700-1−1700-5.

(12) Weiner, S.; Sagi, I.; Addadi, L. Choosing the Crystallization Path Less Traveled. *Science* **2005**, *309*, 1027−1028.

(13) Dorozhkin, S. V.; Epple, M. Biological and Medical Significance of Calcium Phosphates. *Angew. Chem., Int. Ed.* **2002**, *41*, 3130−3146.

(14) Tang, Q. L.; Zhu, Y. J.; Wu, J.; Chen, F.; Cao, S. W. Calcium Phosphate Drug Nanocarriers with Ultrahigh and Adjustable Drug-Loading Capacity: One-Step Synthesis, in Situ Drug Loading and Prolonged Drug Release. *Nanomed.—Nanotechnol.* **2011**, *7*, 428−434.

(15) Wang, K. W.; Zhou, L. Z.; Sun, Y.; Wu, G. J.; Gu, H. C.; Duan, Y. R.; Chen, F.; Zhu, Y. J. Calcium Phosphate/PLGA-mPEG Hybrid Porous Nanospheres: A Promising Vector with Ultrahigh Gene Loading and Transfection Efficiency. *J. Mater. Chem.* **2010**, *20*, 1161−1166.

(16) Wang, K. W.; Zhu, Y. J.; Chen, X. Y.; Zhai, W. Y.; Wang, Q.; Chen, F.; Chang, J.; Duan, Y. R. Flower-Like Hierarchically Nanostructured Hydroxyapatite Hollow Spheres: Facile Preparation and Application in Anticancer Drug Cellular Delivery. *Chem.—Asian J.* **2010**, *5*, 2477−2482.

(17) Wu, G. J.; Zhou, L. Z.; Wang, K. W.; Chen, F.; Sun, Y.; Duan, Y. R.; Zhu, Y. J.; Gu, H. C. Hydroxylapatite Nanorods: An Efficient and Promising Carrier for Gene Transfection. *J. Colloid Interface Sci.* **2010**, *345*, 427−432.

(18) Qiu, N.; Yin, H.; Ji, B.; Klauke, N.; Glidle, A.; Zhang, Y. K.; Song, H.; Cai, L. L.; Ma, L.; Wang, G. C.; Chen, L. J.; Wang, W. W. Calcium Carbonate Microspheres as Carriers for the Anticancer Drug Camptothecin. *Mater. Sci. Eng., C* **2012**, *32*, 2634−2640.

(19) Wei, W.; Ma, G. H.; Hu, G.; Yu, D.; Mcleish, T.; Su, Z. G.; Shen, Z. Y. Preparation of Hierarchical Hollow $CaCO_3$ Particles and the Application as Anticancer Drug Carrier. *J. Am. Chem. Soc.* **2008**, *130*, 15808−15810.

(20) Hou, Z. Y.; Yang, P. P.; Lian, H. Z.; Wang, L. L.; Zhang, C. M.; Li, C. X.; Chai, R. T.; Cheng, Z. Y.; Lin, J. Multifunctional Hydroxyapatite Nanofibers and Microbelts as Drug Carriers. *Chem.—Eur. J.* **2009**, *15*, 6973−6982.

(21) Zhou, H.; Lee, J. Nanoscale Hydroxyapatite Particles for Bone Tissue Engineering. *Acta Biomater.* **2011**, *7*, 2769−2781.

(22) Suchanek, W.; Yoshimura, M. Processing and Properties of Hydroxyapatite-Based Biomaterials for Use as Hard Tissue Replacement Implants. *J. Mater. Res.* **1998**, *13*, 94−117.

(23) Chen, F.; Huang, P.; Zhu, Y. J.; Wu, J.; Zhang, C. L.; Cui, D. X. The Photoluminescence, Drug Delivery and Imaging Properties of Multifunctional Eu^{3+}/Gd^{3+} Dual-Doped Hydroxyapatite Nanorods. *Biomaterials* **2011**, *32*, 9031−9039.

(24) Chen, F.; Zhu, Y. J.; Zhang, K. H.; Wu, J.; Wang, K. W.; Tang, Q. L.; Mo, X. M. Europium-Doped Amorphous Calcium Phosphate Porous Nanospheres: Preparation and Application as Luminescent Drug Carriers. *Nanoscale Res. Lett.* **2011**, *6*, 67−75.

(25) Yang, P. P.; Quan, Z. W.; Li, C. X.; Kang, X. J.; Lian, H. Z.; Lin, J. Bioactive, Luminescent and Mesoporous Europium-Doped Hydroxyapatite as a Drug Carrier. *Biomaterials* **2008**, *29*, 4341−4347.

(26) Zhang, C. M.; Li, C. X.; Huang, S. S.; Hou, Z. Y.; Cheng, Z. Y.; Yang, P. P.; Peng, C.; Lin, J. Self-Activated Luminescent and Mesoporous Strontium Hydroxyapatite Nanorods for Drug Delivery. *Biomaterials* **2010**, *31*, 3374−3383.

(27) Zhao, X. Y.; Zhu, Y. J.; Chen, F.; Lu, B. Q.; Qi, C.; Zhao, J.; Wu, J. Hydrothermal Synthesis of Hydroxyapatite Nanorods and Nanowires Using Riboflavin-5′-phosphate Monosodium Salt as a New Phosphorus Source and Their Application in Protein Adsorption. *CrystEngComm* **2013**, *15*, 7926−7935.

(28) Qi, C.; Zhu, Y. J.; Lu, B. Q.; Zhao, X. Y.; Zhao, J.; Chen, F. Hydroxyapatite Nanosheet-Assembled Porous Hollow Microspheres: DNA-Templated Hydrothermal Synthesis, Drug Delivery and Protein Adsorption. *J. Mater. Chem.* **2012**, *22*, 22642−22650.

(29) Kim, Y.-Y.; Hetherington, N. B. J.; Noel, E. H.; Kröger, R.; Charnock, J. M.; Christenson, H. K.; Meldrum, F. C. Capillarity Creates Single-Crystal Calcite Nanowires from Amorphous Calcium Carbonate. *Angew. Chem., Int. Ed.* **2011**, *50*, 12572−12577.

(30) Gebauer, D.; Gunawidjaja, P. N.; Ko, J. Y. P.; Bacsik, Z.; Aziz, B.; Liu, L.; Hu, Y.; Bergström, L.; Tai, C.-W.; Sham, T.-K.; Edén, M.; Hedin, N. Proto-Calcite and Proto-Vaterite in Amorphous Calcium Carbonates. *Angew. Chem., Int. Ed.* **2010**, *49*, 8889−8891.

(31) Eanes, E. D.; Termine, J. D.; Nylen, M. U. An Electron Microscopic Study of the Formation of Amorphous Calcium Phosphate and Its Transformation to Crystalline Apatite. *Calcif. Tissue Res.* **1973**, *12*, 143−158.

(32) Meiron, O. E.; Bar-David, E.; Aflalo, E. D.; Shechter, A.; Stepensky, D.; Berman, A.; Sagi, A. Solubility and Bioavailability of

Stabilized Amorphous Calcium Carbonate. *J. Bone Miner. Res.* **2011**, *26*, 364−372.
(33) Nagano, M.; Nakamura, T.; Kokubo, T.; Tanahashi, M.; Ogawa, M. Differences of Bone Bonding Ability and Degradation Behaviour in Vivo Between Amorphous Calcium Phosphate and Highly Crystalline Hydroxyapatite Coating. *Biomaterials* **1996**, *17*, 1771−1777.
(34) Balasundaram, G.; Sato, M.; Webster, T. J. Using Hydroxyapatite Nanoparticles and Decreased Crystallinity To Promote Osteoblast Adhesion Similar to Functionalizing with RGD. *Biomaterials* **2006**, *27*, 2798−2805.
(35) Michel, F. M.; MacDonald, J.; Feng, J.; Phillips, B. L.; Ehm, L.; Tarabrella, C.; Parise, J. B.; Reeder, R. J. Structural Characteristics of Synthetic Amorphous Calcium Carbonate. *Chem. Mater.* **2008**, *20*, 4720−4728.
(36) Boskey, A. L.; Posner, A. S. Conversion of Amorphous Calcium Phosphate to Microcrystalline Hydroxyapatite. A pH-Dependent, Solution-Mediated, Solid-Solid Conversion. *J. Phys. Chem.* **1973**, *77*, 2313−2317.
(37) Sato, A.; Nagasaka, S.; Furihata, K.; Nagata, S.; Arai, I.; Saruwatari, K.; Kogure, T.; Sakuda, S.; Nagasawa, H. Glycolytic Intermediates Induce Amorphous Calcium Carbonate Formation in Crustaceans. *Nat. Chem. Biol.* **2011**, *7*, 197−199.
(38) Wolf, S. E.; Leiterer, J.; Pipich, V.; Barrea, R.; Emmerling, F.; Tremel, W. Strong Stabilization of Amorphous Calcium Carbonate Emulsion by Ovalbumin: Gaining Insight into the Mechanism of 'Polymer-Induced Liquid Precursor' Processes. *J. Am. Chem. Soc.* **2011**, *133*, 12642−12649.
(39) Aizenberg, J.; Lambert, G.; Addadi, L.; Weiner, S. Stabilization of Amorphous Calcium Carbonate by Specialized Macromolecules in Biological and Synthetic Precipitates. *Adv. Mater.* **1996**, *8*, 222−226.
(40) Faatz, M.; Gröhn, F.; Wegner, G. Amorphous Calcium Carbonate: Synthesis and Potential Intermediate in Biomineralization. *Adv. Mater.* **2004**, *12*, 996−1000.
(41) Aizenberg, J.; Lambert, G.; Weiner, S.; Addadi, L. Factors Involved in the Formation of Amorphous and Crystalline Calcium Carbonate: A Study of an Ascidian Skeleton. *J. Am. Chem. Soc.* **2002**, *124*, 32−39.
(42) Gal, A.; Hirsch, A.; Siegel, S.; Li, C.; Aichmayer, B.; Politi, Y.; Fratzl, P.; Weiner, S.; Addadi, L. Plant Cystoliths: A Complex Functional Biocomposite of Four Distinct Silica and Amorphous Calcium Carbonate Phases. *Chem.—Eur. J.* **2012**, *18*, 10262−10270.
(43) Ihli, J.; Kim, Y.-Y.; Noel, E. H.; Meldrum, F. C. The Effect of Additives on Amorphous Calcium Carbonate (ACC): Janus Behavior in Solution and the Solid State. *Adv. Funct. Mater.* **2013**, *23*, 1575−1585.
(44) Liu, J.; Pancera, S.; Boyko, V.; Gummel, J.; Nayuk, R.; Huber, K. Impact of Sodium Polyacrylate on the Amorphous Calcium Carbonate Formation from Supersaturated Solution. *Langmuir* **2012**, *28*, 3593−3605.
(45) Cai, G. B.; Zhao, G. X.; Wang, X. K.; Yu, S. H. Synthesis of Polyacrylic Acid Stabilized Amorphous Calcium Carbonate Nanoparticles and Their Application for Removal of Toxic Heavy Metal Ions in Water. *J. Phys. Chem. C* **2010**, *114*, 12948−12954.
(46) Bassett, D. C.; Marelli, B.; Nazhat, S. N.; Barralet, J. E. Stabilization of Amorphous Calcium Carbonate with Nanofibrillar Biopolymers. *Adv. Funct. Mater.* **2012**, *22*, 3460−3469.
(47) Li, Y. B.; Weng, W. J. In Vitro Synthesis and Characterization of Amorphous Calcium Phosphates with Various Ca/P Atomic Ratios. *J. Mater. Sci.: Mater. Med.* **2007**, *18*, 2303−2308.
(48) Tang, Q. L.; Zhu, Y. J.; Duan, Y. R.; Wang, Q.; Wang, K. W.; Cao, S. W.; Chen, F.; Wu, J. Porous Nanocomposites of PEG-PLA/Calcium Phosphate: Room-Temperature Synthesis and Its Application in Drug Delivery. *Dalton Trans.* **2010**, *39*, 4435−4439.
(49) Politi, Y.; Batchelor, D. R.; Zaslansky, P.; Chmelka, B. F.; Weaver, J. C.; Sagi, I.; Weiner, S.; Addadi, L. Role of Magnesium Ion in the Stabilization of Biogenic Amorphous Calcium Carbonate: A Structure−Function Investigation. *Chem. Mater.* **2010**, *22*, 161−166.
(50) Rodriguez-Blanco, J. D.; Shaw, S.; Bots, P.; Roncal-Herrero, T.; Benning, L. G. The Role of pH and Mg on the Stability and Crystallization of Amorphous Calcium Carbonate. *J. Alloys Compd.* **2012**, *536S*, S477−S479.
(51) Kellermeier, M.; Melero-García, E.; Glaab, F.; Klein, R.; Drechsler, M.; Rachel, R.; García-Ruiz, J. M.; Kunz, W. Stabilization of Amorphous Calcium Carbonate in Inorganic Silica-Rich Environments. *J. Am. Chem. Soc.* **2010**, *132*, 17859−17866.
(52) Gal, A.; Weiner, S.; Addadi, L. The Stabilizing Effect of Silicate on Biogenic and Synthetic Amorphous Calcium Carbonate. *J. Am. Chem. Soc.* **2010**, *132*, 13208−13211.
(53) Blumenthal, N. C.; Betts, F.; Posner, A. S. Stabilization of Amorphous Calcium Phosphate by Mg and ATP. *Calcif. Tissue Res.* **1977**, *23*, 245−250.
(54) Gedye, R.; Smith, F.; Westaway, K.; Ali, H.; Baldisera, L.; Laberge, L.; Rousell, J. The Use of Microwave Ovens for Rapid Organic Synthesis. *Tetrahedron Lett.* **1986**, *27*, 279−282.
(55) Giguere, R. J.; Bray, T. L.; Duncan, S. M.; Majctich, G. Application of Commercial Microwave Ovens to Organic Synthesis. *Tetrahedron Lett.* **1986**, *27*, 4945−4948.
(56) Tsuji, M.; Hashimoto, M.; Nishizawa, Y.; Kubokawa, M.; Tsuji, T. Microwave-Assisted Synthesis of Metallic Nanostructures in Solution. *Chem.—Eur. J.* **2005**, *11*, 440−452.
(57) Zhu, Y. J.; Wang, W. W.; Qi, R. J.; Hu, X. L. Microwave-Assisted Synthesis of Single-Crystalline Tellurium Nanorods and Nanowires in Ionic Liquids. *Angew. Chem., Int. Ed.* **2004**, *43*, 1410−1414.
(58) Abolinš-Krogis, A. The Effect of Adenosine Triphosphate, Magnesium Chloride and Phospholipids on Crystal Formation in the Demineralized Shell-Repair Membrane of the Snail, Helix Pomatia L. *Cell Tissue Res.* **1979**, *204*, 497−505.
(59) Qi, C.; Zhu, Y. J.; Zhao, X. Y.; Lu, B. Q.; Tang, Q. L.; Zhao, J.; Chen, F. Highly Stable Amorphous Calcium Phosphate Porous Nanospheres: Microwave-Assisted Rapid Synthesis Using ATP as Phosphorus Source and Stabilizer, and Their Application in Anticancer Drug Delivery. *Chem.—Eur. J.* **2013**, *19*, 981−987.
(60) Posner, A. S.; Betts, F.; Blumenthal, N. C. Role of ATP and Mg in the Stabilization of Biological and Synthetic Amorphous Calcium Phosphates. *Calcif. Tissue Res.* **1976**, *22*, 208−212.
(61) Oaki, Y.; Kajiyama, S.; Nishimura, T.; Imai, H.; Kato, T. Nanosegregated Amorphous Composites of Calcium Carbonate and an Organic Polymer. *Adv. Mater.* **2008**, *20*, 3633−3637.
(62) Zhang, Z. N.; Xie, Y. D.; Xu, X. R.; Pan, H. H.; Tang, R. K. Transformation of Amorphous Calcium Carbonate into Aragonite. *J. Cryst. Growth* **2012**, *343*, 62−67.
(63) Qi, C.; Zhu, Y. J.; Chen, F. Fructose 1,6-Bisphosphate Trisodium Salt as a New Phosphorus Source for the Rapid Microwave Synthesis of Porous Calcium−Phosphate Microspheres and Their Application in Drug Delivery. *Chem.—Asian J.* **2013**, *8*, 88−94.
(64) Qi, C.; Tang, Q. L.; Zhu, Y. J.; Zhao, X. Y.; Chen, F. Microwave-Assisted Hydrothermal Rapid Synthesis of Hydroxyapatite Nanowires Using Adenosine 5′-Triphosphate Disodium Salt as Phosphorus Source. *Mater. Lett.* **2012**, *85*, 71−73.
(65) Qi, C.; Zhu, Y. J.; Lu, B. Q.; Zhao, X. Y.; Zhao, J.; Chen, F.; Wu, J. Hydroxyapatite Hierarchically Nanostructured Porous Hollow Microspheres: Rapid, Sustainable Microwave-Hydrothermal Synthesis by Using Creatine Phosphate as an Organic Phosphorus Source and Application in Drug Delivery and Protein Adsorption. *Chem.—Eur. J.* **2013**, *19*, 5332−5341.
(66) Gao, W.; Sha, B. Y.; Zou, W.; Liang, X.; Meng, X. Z.; Xu, H.; Tang, J.; Wu, D. C.; Xu, L. X.; Zhang, H. Cationic Amylose-Encapsulated Bovine Hemoglobin as a Nanosized Oxygen Carrier. *Biomaterials* **2011**, *32*, 9425−9433.